DOI: 10.15480/882.9367

Eighth International Symposium on Marine Propulsors
smp'24, Berlin, Germany, March 2024

Derivation of a numerical propeller-ice interaction model

Angelo Mario Böhm[1], **Lina Sapp**[1], **Franz von Bock und Polach**[1]

[1]Institute for Ship Structural Design and Analysis, Hamburg University of Technology, Hamburg, Germany

ABSTRACT

Ice is a strain rate-dependent material showing ductile and brittle behavior and can play a critical role in maritime operations. Particularly in propeller-ice interactions, with high strain rates, ice fails brittle. Such interactions not only induce potential damage to the propeller, but also have a significant impact on the entire drive train of vessels in ice. The determination of ice-induced loads on propellers is a significant challenge, as direct measurements are usually not possible and indirect measurements are contaminated and superimposed with various other signals.

Therefore, this paper delves into the domain of dynamic finite element simulations focusing on the interaction between ice and ship propellers in connection with dedicated small scale experiments.

Experiments emulating propeller-ice milling-type interactions have been employed to enhance the knowledge of propeller-ice interaction and ice as a material. These experiments serve as input to refine the numerical model, which is a state-of-the-art Mohr-Coulomb Nodal Split (MCNS) ice material model.

The aim is to determine the ice loading on the propeller numerically and to compare the experimental results with the simulation. These simulations in combination with the experiments provide insight into complex propeller-ice dynamics and enable investigating the applicability of the MCNS model for propeller-ice simulations. The discussion includes the observed phenomena, emphasizing the propagation of brittle fractures and their effects on the propeller.

In summary, this study comprehensively explores propeller-ice interactions through finite element simulations. This research contributes to the understanding of ice-induced mechanical challenges in the maritime realm by considering the brittle behavior of ice.

Keywords

propeller-ice interaction, finite element simulations, brittle behavior, maritime operations, ice material model

1 INTRODUCTION

The propulsion systems of vessels in ice are exposed to loads due to propeller-ice contact. Between 2011 and 2020, 240 machinery damages and failures were reported (Allianz Global Corporate and Specialty 2021) in the Arctic Circle waters. This is more than 45% of all incidents in arctic waters. A better understanding of the propeller-ice interaction process allows a more efficient propeller design and a safer operation in ice-covered waters. Despite the loads on the hull of a ship having been measured multiple times in the past by, e.g., Hoffmann (1985), Kujala et al. (2009), Suominen et al. (2013), Suominen (2018), and being calculable to some extent, the direct measurement of propeller-ice loads is not possible.

Propeller-ice loads are commonly divided into contact loads, where milling loads and impact loads are categorized, and non-contact loads, where hydrodynamic loads and hydrodynamic blockage are categorized. Propeller milling loads occur when the leading propeller edge cuts into the ice. At impact loads the ice hits the propeller face, but is not contacted or cut by the leading edge. Hydrodynamic loads are all loads that do not involve influences due to contact with ice. At hydrodynamic blockage, the ice does not contact the propeller. Still, it is close enough to affect the flow around the propeller and, thereby, the hydrodynamic load. The flow of the water could also be affected such that cavitation occurs, which increases the hydrodynamic load to a great extent. This work focuses on the milling loads.

An analytical model to describe the milling process during propeller-ice interaction was developed by Veitch (1995), assuming the propeller to be a rigid body. He also concluded that the direct contact loads are significantly higher than any hydrodynamic loads resulting from blockage, and that the effects of ice motion should be incorporated into any simulation model of the propeller-ice interaction process. Furthermore, the knowledge about ice contact and ice failure mechanics from experiments using model edges done by, e.g., Belyashov (1993, 1995) should be extended by experiments using propeller edges. The propeller-ice interaction was also described on a model scale and validated against full-scale measurements by Soininen (1998), and he simulated among the first the propeller-ice interaction process. Soininen (1998) concluded that the mechanism of spall formation versus local crushing requires further research. Although novel approaches to investigate propeller-ice interaction exist, for example, the use of peridynamics by Ye et al. (2017), the original investigators like Belyashov and Shpakov (1983), Veitch (1995) and Soini-

nen (1998) utilized the Mohr-Coulomb failure criterion for the ice material definition.

The frame-work, to overcome the problem of direct measurements of propeller-ice milling loads, is as follows. Frist, high-impact drop tower experiments with a single propeller blade will be conducted to separate the complex propeller-ice interaction process of an ice-going vessel from the hydrodynamic loads. This enables a direct experimental investigation of the propeller-ice interaction process. However, to ensure that enough load is transferred into the propeller edges without causing damage to the propellers or the drop tower, information about the dynamics of the drop hammer, the load transfer of the laboratory-made ice with high compressive strength, and the failure behavior of the ice is needed.

The forces and failure patterns in experiments with a model edge and a compression testing machine on a low-speed scale of about 0.2 m/s were already described experimentally in (Böhm et al. 2022b), and the presented study is the subsequent investigation within the frame-work.

The presented preliminary study investigates the current experimental setup using a drop tower for high impact velocities and derives reference values using model edges, which mimic propeller edges. In addition, the experiments will be simulated in LS-DYNA using the finite element method (FEM). The simulation will give us a deeper insight into the Mohr-Coulomb Nodal Split (MCNS) model, which was developed and validated by Herrnring (2023) for interaction velocities up to 10 mm/s. When the MCNS model can represent the load transfer and the failure behavior of the ice at higher interaction velocities, the prepended simulations of the propeller edge experiments will assess the dynamics of the experiment for a safe experimental execution. Ultimately, the adjusted MCNS model will be used in propeller-ice simulations, as presented in Figure 1, without considering hydrodynamic loads.

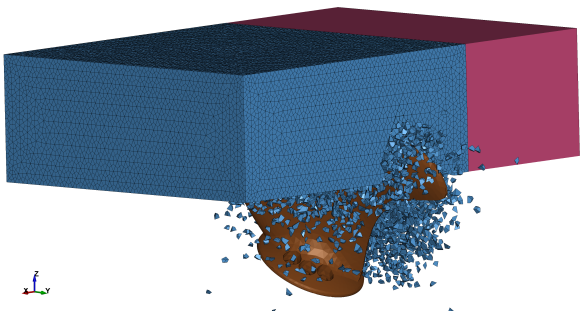

Figure 1: Simulation of a propeller milling into an ice block. The ice block is modeled rigid (red) and with the MCNS model (blue part).

High-performance computing could enable the investigation of a complete propeller-ice interaction process, considering hydrodynamic loads, with the adjusted MCNS model.

Besides presenting the experimental results of high-speed drop tower tests of ice with model edges, which mimic propeller edges, the paper investigates the following research question: Can the Mohr-Coulomb Nodal Split model be applied to the numerical investigation of propeller-ice interaction?

2 EXPERIMENTS

This section describes the ice specimen preparation, the experimental setup, and the execution of the experiments.

2.1 Specimen Preparation

The ice specimen geometry for testing is a cylinder with a length of 250 mm and a diameter of 99.4 mm. The ice specimen production has been established at the Institute for Ship Structural Design and Analysis at the Hamburg University of Technology for several years (Herrnring et al. 2017; Herrnring et al. 2020; Böhm et al. 2022a; Müller et al. 2023). The key components for the ice specimen preparation are commercially available crushed ice, distilled water, PVC-U pipes, aluminum plates, and insulating material. Further, a cooling container or chamber, a large ice crushing machine, a hot air gun, a cutter, and a saw are needed.

First, the aluminum plate is glued with silicone to the PVC-U pipe and stored in a dry environment until the silicone dries. When the silicon is dry the preparation of the ice specimen can start in the cooling container. Therefore, the commercial available crushed ice is crushed further with a large ice crushing machine, ensuring a homogeneous bulk. Then we filled 2/3 of the PVC-U with the ice, 1/3 with distilled water and stirred the mix of water and crushed ice to reduce air pockets. At the end of the preparation, the PVC-U pipe is closed with an insulating lid. The aluminum plate at the bottom results in a freezing process from bottom to top. The ice specimens for this paper froze for two days at - 10 °C. After freezing, the ice specimen is removed from the PVC-U pipe by removing the aluminum plate with a cutter and pushing out the ice specimen of the PVC-U pipe with the help of a hot air gun. The hot air gun heated the pipe for a short time, so that the ice specimen could loosen. After the removal, the ice specimen is cut into the desired length.

This procedure led to a granular grain structure with a grain size of about 1.5 mm (Böhm et al. 2022a), which was determined by linear intercept method (Herrnring 2023). Our laboratory-made ice is granular freshwater ice with a strength equivalent to glacial ice and consequently higher than for sea ice (Timco and Weeks 2010), which will lead to conservative results.

2.2 Experimental Setup and Execution

The experimental setup consists of a drop tower, the ice specimen mounted to the drop hammer with a specimen holder, the propeller blade edge model, a heavy lift crane, an emergency release hook, a high-speed camera, and a measuring system, see Figure 2.

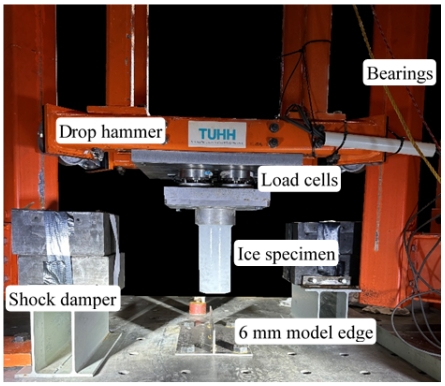

Figure 2: Drop tower with ice specimen and 6 mm propeller blade edge model. The measuring system stands by the drop tower.

For the execution of the experiments, first, the ice specimen has to be frozen within the specimen holder using a thin layer of water as adhesive. The freezing process takes about one to five minutes as the specimen holder is cooled days before the execution of the experiments. In the meantime, the drop hammer is lifted from the shock dampers with a large enough gap that ensures bolting the specimen holder with the ice specimen to the drop hammer properly. When the ice specimen with the specimen holder is bolted to the drop hammer, the desired interaction velocity is adjusted through the travel distance of the ice specimen. Load cells between the drop hammer and the specimen holder measure the interaction force. The interaction velocity in this study is 3 m/s, 4 m/s or 5 m/s to investigate its dependency on the measured force. The drop height can be calculated analytically by considering the principle of conservation of energy as Equations 1-2 show:

$$E = mgh = 1/2mv^2 = \text{constant} \tag{1}$$

$$h = v^2/2g \tag{2}$$

The experiment starts when the measurements and the high-speed camera are started to record the interaction force, the movement of the drop hammer, and the failure behavior of the ice specimen. After the emergency release hook is released, the drop hammer falls with the ice specimen and hits the model edge. The interaction process lasts a few milliseconds. To investigate the size effect of the model edge, 3 mm and 6 mm wide model edges were used. Additionally, the edge is rounded off to have a more defined contact between the ice specimen and the blade edge model. The shock dampers absorb the residual energy of the drop hammer after the impact, and after a few seconds, the drop hammer stops moving, which ends the experiment. Removing the ice debris and drying the drop tower is mandatory for safe follow-up experiments.

3 SIMULATION SETUP AND MCNS MODEL

This chapter explains the simulation setup and the Mohr-Coulomb Nodal Split (MCNS) ice material model, including relevant parameters and assumptions.

Figure 3 shows the simulation model, including the drop hammer, the load cells, the specimen holder, the ice specimen, and the model edge fixed on the foundation. The drop hammer model and the foundation model are a detailed representation of the experimental setup in the laboratory and consist of Belytschko-Tsay shell elements and fully integrated S/R solid elements. The simulation model of the drop hammer and the foundation has no holes or screws, and the drop hammer model has no wheels. The resulting reduction in weight of the drop hammer model compared to the build drop hammer (approximately 23 kg) was compensated by increasing the density of the drop hammer model from 7850 kg/m^3 by 11.7%. The bearing of the drop hammer is realized by applying translational constraints in the plane perpendicular to the falling direction. The material for the drop hammer and the foundation is steel.

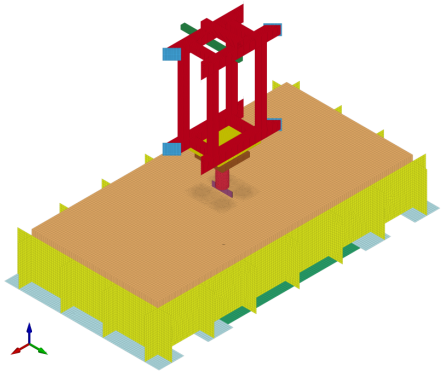

Figure 3: Isometric view of the simulation setup in LS-DYNA.

Except for the model edge, the ice specimen, and the load cells, a material model capable of representing kinematic hardening plasticity is used. The model edge is modeled as a rigid material, a common practice in propeller-ice interaction investigations (Kotras et al. 1987; Soininen 1998; Ye et al. 2017; Wang et al. 2018; Xiong et al. 2020). The use of a rigid material formulation reduces the computational time significantly. However, other than that, the model edge is also a detailed representation of the build edges, including the rounding of the edge, as Figure 4 shows.

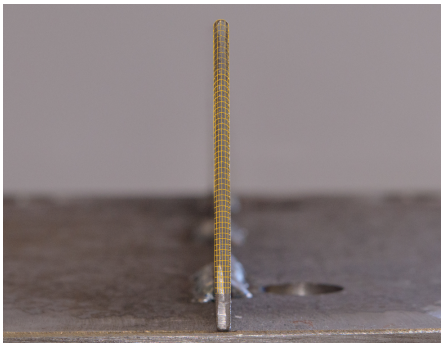

Figure 4: The finite element mesh in yellow is placed on the photo of the 6 mm model edge.

The load cells are modeled as discrete springs and discrete viscous dampers, whereas the stiffness of the spring is set to the stiffness of the load cell taken from its technical documentation. In a preliminary parameter study, the spring and

damping coefficients were fine-tuned using an aluminum cylinder as a testing object. Gravity is added in the vertical direction, and the vertical translation of the bottom of the foundation is constrained. The drop hammer with the load cells and the ice specimen within the specimen holder are set right above the model edge and subjected to an initial velocity of 3 m/s, 4 m/s or 5 m/s in order to save computational time. For the ice material the MCNS model is used, which is a finite element model that combines the elastic ideal-plastic Mohr-Coulomb material model with the nodal splitting method and is based on Herrnring (2023). The Mohr-Coulomb theory puts the shear and normal stress at failure into relation. The nodal splitting method represents the failure model and allows elements to detach from their neighbor elements because the nodes of every element are independent of the neighbor element. Couplings between nodes are established using kinematic couplings. They are removed when the volume-weighted plastic strain in neighboring elements exceeds a critical value of 0.002 (0.2%), which is more a value for numerical stability than representing the actual failure behavior of the ice material (Herrnring et al. 2022). However, the nodal splitting method maintains mass conservation compared to erosion techniques. The MCNS model for the ice specimen has a hexahedral mesh of fully integrated S/R solid elements for poor aspect ratios. S/R stands for selective reduced integration and is a technique in FEM where some integration points are removed to reduce computational costs. Thus, a fully integrated S/R solid element combines both full integration for some integration points while selectively reducing integration points to achieve a compromise between accuracy and computational efficiency. Table 1 shows the parameters for granular freshwater ice at approximately -10° C for the ice material model.

Table 1: Material parameters for granular freshwater ice at -10° C.

Density	900	kg/m^3
Elastic shear modulus	3.5	GPa
Poisson's ratio	0.33	-
Angle of friction	0.526	rad
Cohesion value	1.5	MPa
Ice-ice friction coefficient	0.05	-
Element size	12.5	mm

In addition, pressure melting is represented in the MCNS model by element erosion and starts at 100 MPa. The model uses the same contact settings for the ice self-contact as proposed by Herrnring (2023), which is contact automatic single surface with the following settings: SOFT = 2, SBOPT = 5, DEPTH = 5, VDC = 20, DTSTIF = $1{\cdot}10^{-6}$. The contact stiffness is a function of the element size and should be reduced to SFS = 0.2 for the element size of 50 mm. Furthermore, for the contact of the model edge and the foundation with the ice specimen, we used contact automatic surface to surface with a value for the static coefficient of friction of 0.03 and the same settings as for automatic single surface for the ice self-contact.

4 RESULTS

This section describes the results of the experiments and the results of the dynamic finite element simulation.

4.1 Experimental results

In total 18 drop tower experiments were conducted resulting in three repetitions for every interaction velocity and thus in 9 test for each model edge. The scatter plot shows the measured first force peak of the load curve versus the interaction velocity for the experiments as well as for the simulation with the 3 mm and 6 mm model edge, see Figure 5. The results of the simulation will be described in the next section.

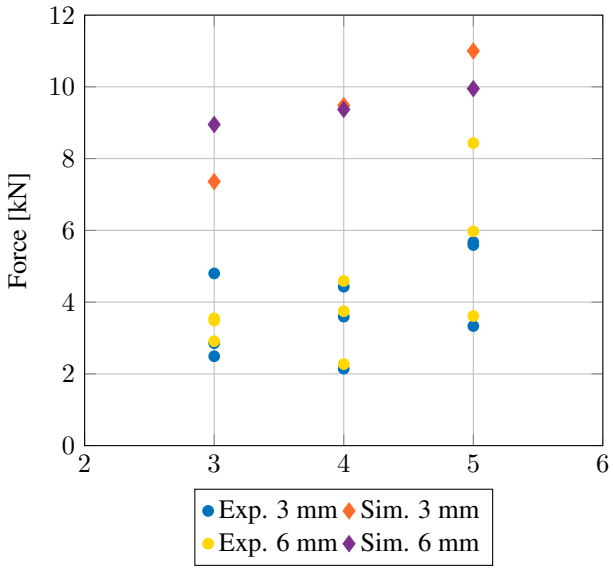

Figure 5: Scatter plot of the first force peak versus interaction velocity for the experiments and the simulations with blades of 3 mm and 6 mm thickness.

For the 3 mm edge, we conducted tests at varying interaction velocities, namely 3 m/s, 4 m/s, and 5 m/s. While the small sample size prevents a robust assessment of variability using confidence intervals or standard deviation, it is evident that the measured first force peak shows some degree of variability. At an interaction velocity of 3 m/s, the measured forces were 2.86 kN, 4.80 kN, and 2.49 kN, with a range of 2.33 kN between the minimum and maximum values. When the interaction velocity increased to 4 m/s, the measured forces were 4.43 kN, 2.14 kN, and 3.60 kN, with a range of 2.29 kN between the minimum and maximum values, suggesting a similar level of variability compared to the 3 m/s tests. At the highest interaction velocity of 5 m/s, the observed forces were 5.67 kN, 3.33 kN, and 5.59 kN, with a range of 2.34 kN between the minimum and maximum values.

For the interaction velocity of 3 m/s for the 6 mm edge the measurements yielded into the following results: 3.55 kN, 3.48 kN, and 2.91 kN with a range of 0.64 kN between the minimum and maximum values. For the interaction velocity of 4 m/s for the 6 mm edge the force measurements yielded into 3.75 kN, 4.59 kN, and 2.27 kN. The difference

between the maximum measured force and the minimum measured force is 2.32 kN. For the interaction velocity of 5 m/s for the 6 mm edge the force measurements yielded into 5.97 kN, 8.43 kN, and 3.61 kN. The degree of variability is higher for the interaction velocity of 5 m/s, with a range of 4.82 kN between the minimum and maximum values.

We will focus our analysis on the experiment, which results in the highest measured force. This approach aligns with our goal of deriving a numerical propeller-ice interaction model that prioritizes a conservative yet realistic representation. In our case, the 6 mm model edge tested with an interaction velocity of 5 m/s resulted in the highest measured force of 8.43 kN and Figure 6 shows the failure behavior of the ice specimen from A – D in sequence.

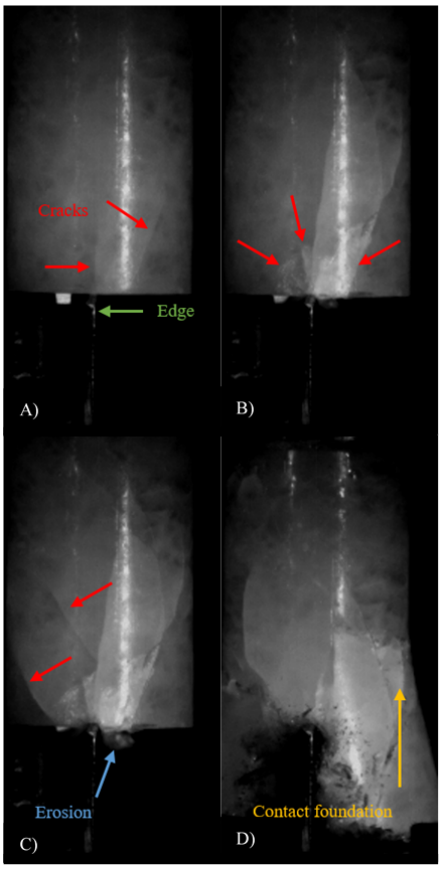

Figure 6: Failure behavior of the ice specimen tested at a velocity of 5 m/s with the 6 mm model edge.

Figure 6 shows four pictures of the failure process and for this experiment the high-speed camera took 10,000 pictures per second. This results in about 130 pictures from the initial contact of the ice specimen with the model edge to the contact of the broken ice specimen with the foundation of the model edge. Figure 6A shows the ice specimen in contact with the 6 mm model edge. Two axial cracks develop. One crack develops right at the contact point and is nearly vertical and the second axial crack is about one centimeter away from the contact point and grows at an angle. Figure 6B, which is 0.3 ms (or three pictures) apart from Figure 6A, shows that the defects increase rapidly and a local crushing zone emerges in an area around the contact point with a diameter of three centimeters. Figure 6C is again 0.3 ms apart from Figure 6B and shows the development of more axial cracks. Some of them spread from the initial cracks and the erosion of the ice material is more visible than in Figure 6B. Figure 6D shows the end of the experiment, where the remaining ice specimen contacts the foundation of the model edge. If the load can be transferred through the remaining ice specimen, it might be that the measured force at this time is higher than the initial force since the contact area is several magnitudes higher than that in the initial contact condition.

4.2 Simulation results

For every model edge (3 mm and 6 mm) three simulations were conducted with an initial velocity of 3 m/s, 4 m/s, or 5 m/s respectively. In Figure 5, the first contact peak force between the model edge versus the initial velocity is shown. In general, the simulation produces higher maximum forces than what was measured in the related experiments. For the simulation with an initial velocity of 3 m/s the first contact peak force is 8.95 kN for the 6 mm model edge and 7.36 kN for the 3 mm model edge (Δ 1.59 kN). For the simulation with an initial velocity of 4 m/s the first contact peak force is 9.37 kN for the 6 mm model edge and 9.48 kN for the 3 mm model edge (Δ -0.11 kN). Furthermore, the simulation with an initial velocity of 5 m/s has a first contact peak force of 9.95 kN for the 6 mm model edge and 11 kN for the 3 mm model edge (Δ -1.05 kN). The first contact peak force is increasing with increasing velocities, but the incline for the 3 mm model edge is higher which results for the highest velocity in a higher force for the 3 mm model edge than for the 6 mm model edge. Nevertheless, because we focus the analysis on the experiment which resulted in the highest forces, we will compare in Figure 7 the experiment with the 6 mm model edge with the respective simulation in more detail.

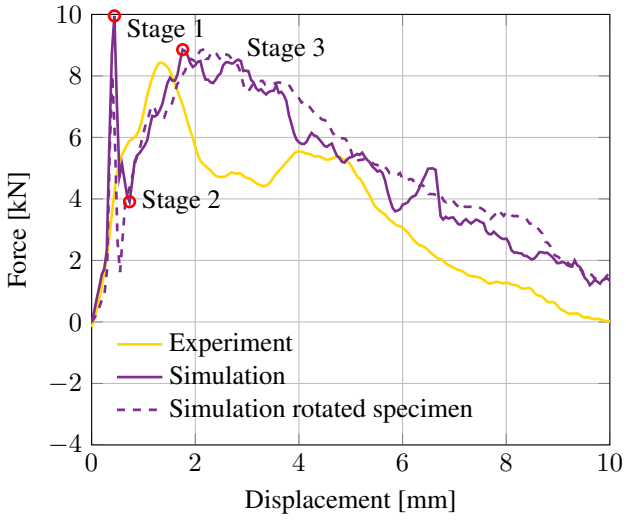

Figure 7: Force versus displacement curve for the 6 mm model edge tested at an impact velocity of 5 m/s.

Figure 7 shows the force versus displacement curves for the experiment (yellow line) and simulation (purple line) with the 6 mm model edge at 5 m/s. The dashed purple line represents a simulation, where one of the outer longitudinal edges of the ice specimen's mesh is in line with the model edge. The impact of this will be reviewed later in Section 5.

Until a displacement of 0.4 mm the force of the simulation increases rapidly to its maximum of 9.95 kN, see Stage 1 in Figure 7. Afterwards it dips to 3.91 kN at a displacement of 0.7 mm, see Stage 2 in Figure 7, and increases again and reaches a second peak of 8.85 kN at a displacement of 1.8 mm, see Stage 3 in Figure 7. The experiment shows a maximum force of 8.43 kN at a displacement of 1.3 mm. Despite the peak force at 0.4 mm, the force-displacement curve of the simulation is similar to that of the experiment. The difference between the simulation and the experiment starts to increase above a displacement of 10 mm. Generally, until a displacement of 10 mm the simulation produces higher forces than the experiment.

Figure 8 shows the failure behavior of the MCNS ice specimen simulated at 5 m/s with the 6 mm model edge.

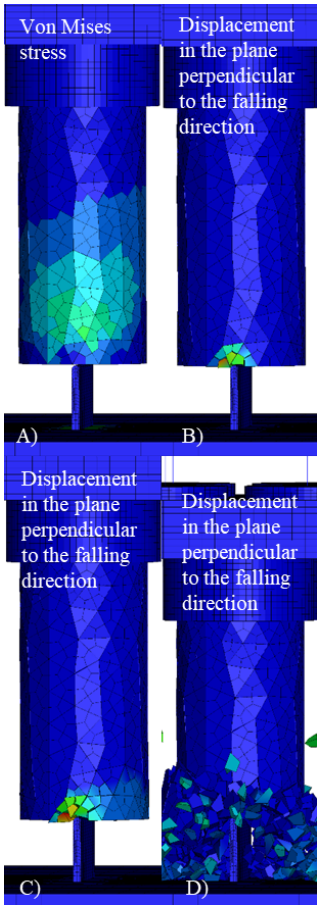

Figure 8: Failure behavior of the MCNS ice specimen simulated at 5 m/s with the 6 mm model edge.

Figure 8A shows the initial contact of the ice specimen with the model edge. To present the initial contact the Von Mises stress is chosen, otherwise there would be nothing visible because there is nearly no movement. In the Figures 8 B-D the representation changed to the displacement in the plane perpendicular to the falling direction. Similar as to Figure 6, Figure 8B is 0.3 ms apart from Figure 8A. Figure 8B shows the local crushing zone with a diameter of three centimeters around the contact point. After another 0.3 ms, see Figure 8C, local material erosion starts at the 6 mm model edge and it is visible that the right edge of the ice comes apart. After 0.01 s the simulations ends, see Figure 8D. The majority of the specimen is still intact, whereby the part of the ice specimen which was penetrated by the model edge disaggregated into element size debris.

5 DISCUSSION

First, we will discuss the capabilities and limitations of the developed experimental setup, including assessing the uncertainty influenced by the ice as a material and the ice specimen preparation technique. The drop tower was already used for the experimental investigation of drop tests with conical ice specimens against full-scale aluminum panels (Herrnring et al. 2017) and drop tests of cylindrical granular ice specimens with different boundary conditions (Böhm et al. 2023). This drop tower setup can adjust the impact energy by the drop height and the mass. Impact velocities up to 6 m/s are possible and the drop hammer can be additionally loaded with up to 1 t. Cylindrical specimens with a diameter of up to 200 mm were already tested (Müller et al. 2023). In the future, the applicability of ice specimens with a diameter of 800 mm is possible, even if this is associated with more significant difficulties in experimental execution. This structural flexibility makes a variety of investigations of high-speed ice-structure interactions at different velocity levels, energy levels, and contact conditions possible. The future experimental setup will consist of scaled propeller edges instead of model edges at different scales, which also aligns with the recommendation from Veitch (1995). However, propeller tip speeds are significantly higher in the range of 25 to 45 m/s for ice-going vessels compared to the initial testing speeds of 3-5 m/s presented here. The drop height restricts the initial testing speed, and overall, the energy output from the experimental setup is limited. Once the numerical models are validated with the existing experiments, the numerical models are expected to account for higher velocities, while it is acknowledged that the extrapolation introduces some uncertainty. The literature review from Timco and Weeks (2010) indicates that milling loads (shear-dominated loads) are less sensitive to the interaction speed for small samples, which suggests that the uncertainty in speed extrapolation might be mitigated. However, comparing simulations with the developed numerical ice material model at higher speeds and reported experiments from the literature could be insightful for future studies. A more significant uncertainty may be, e.g., the missing investigation of the blade edge radius or various ice strengths, yet this is beyond the scope of this paper. Besides these structural capabilities and limitations, the measuring system influences the experiments and their results.

The laser displacement sensor and the acceleration sensor measure the movement of the drop hammer. The nomi-

nal load for each load cell is 100 kN, which sets the maximum measurable force to 400 kN. The measurements are sampled at 100 kHz, sufficient to have a good data resolution, and a lower sample rate is not suggested. Figure 7 highlights that 100 kHz is the lower threshold for the measurement frequency, as there are around 230 data points until a displacement of 10 mm. Furthermore, the summed load signals showed a noise floor of around 300 N, which is a deviation of 14% for the lowest measured force. Nevertheless, the deviation decreases with increasing measured forces. Before every test, the load measurement was checked by measuring the weight of the drop hammer with an additional load cell attached between the energy release hook and the drop hammer to ensure that the load cells were still measuring correctly. The increasing deviation between simulation and experiment above a displacement of 10 mm is result of the high dynamics in the experiments and its influence on the measuring system.

In the processing and analysis of the experimental data, it was not that convenient to extract the exact point of time of the impact between the model edge and the ice specimen because when the ice specimen impacted the foundation of the model edge or when the drop hammer impacted the shock dampers much higher forces were measured compared to the measured forces of the interaction between the model edge and the ice specimen. The high sensitivity of the acceleration signal, combined with the displacement measurement of the drop hammer, was the remedy for extracting the right point of time.

The specimen preparation was conducted with the highest meticulousness. Every contamination or deviation of the preparation procedure can change the structural integrity of the ice specimen. Nonetheless, minor contaminations are inevitable, and as long as the specimens are prepared by the same team in combination with randomizing preparation and testing, the errors are regarded as evenly distributed. Ice is a natural material and behaves at the tested velocity brittle, so a high data scatter is expected. An increase in the number of trials would be necessary to obtain statistically significant results. With the existing scatter, the number of samples would have to be increased by at least ten, if not a hundred times, which was not considered necessary ecologically and economically according to our experience. The accurate sample preparation and execution of the experiments, combined with some repetitions for every velocity level ensured high interaction forces compared to what sea ice could exert on structures. Sea ice is more porous and thus much weaker in its structural integrity than our laboratory-made ice (Timco and Weeks 2010).

Selecting the suitable numerical method and numerical ice material model is essential for deriving a numerical propeller-ice interaction model. The FEM is most well-developed numerical method. It has a significant advantage because of the coupling of the interaction objects (here, ice and structure) utilizing contact algorithms, among other advantages. Herrnring (2023) showed that the developed MCNS ice material model is suitable for large-scale applications as the simulation of brittle experiments with ice specimens with a diameter of 800 mm compressed on a ship hull structure with dimensions of 3 m times 2 m provided similar results compared to the experiments. Also, the simulation of the large double-pendulum ice impact tests with an ice specimen with a diameter of 1 m and an interaction velocity of 4.1 m/s of Gagnon et al. (2020) provided a good fit. Lu et al. (2021) successfully applied smoothed-particle hydrodynamics (SPH) for the ice material in numerical investigations of propeller-ice interaction. However, applying boundary conditions is one of the most challenging parts of the SPH method (Shadloo et al. 2016) and is one of the reasons why it is sparsely used in investigations of propeller-ice interaction. Peridynamics are also very promising regarding fracture models and computational cost in comparison to the FEM for large-scale simulations with fine meshes. Recent propeller-ice simulation using peridynamics can be found, e.g., in (Ye et al. 2017, Ye et al. 2019, Xiong et al. 2020). The theory behind bond-based peridynamics assumes, that each peridynamic bond responds independently of all the other bonds. This assumption implies that any isotropic linear elastic solid is restricted to a Poisson's ratio of 0.25. The typical Poisson's ratio of ice is between 0.30 and 0.33, which means that the simulation using bond-based peridynamics inherently presents different results between milling and impact loads than simulations using the conventional mechanical properties of ice. In general, also other meticulously designed methods, as e.g. the inverse method of de Waal et al. (2018) and Nickerson et al. (2021), the cohesion element method (CEM) of Zhou et al. (2019) or the discrete element method (DEM) of Yang et al. (2023) for the ice material formulation, or the panel method of Wang (2007) and Khan et al. (2020) lead to applicable investigations of propeller-ice interaction in their specific use-case. However, a holistic numerical material formulation for ice is desirable as we have today for steel.

From a theoretical point of view, the future improvements of the MCNS model should include a strain-rate dependency as ice is strain-rate dependent in compression. Nevertheless, it seems that this is less of a problem for milling types of simulations. For the initial contact phase, the mass and stiffness of the specimen are rightfully represented by the MCNS model. After the failure, the nodal splitting approach is handy as the energy entry with continuous ice crushing can be represented. Other models work with the erosion of elements, which reduces the possible energy entry. The disadvantage of the nodal splitting approach is that it increases the number of nodes, and thus, it is directly linked to the computational effort. Moreover, the meshing of the ice and the influence of the triaxiality should be further investigated. Figure 7 showed that the orientation of the ice specimen's mesh influences the interaction process like the grain size and grain structure influences the measured forces and the failure behavior in experiments. The consideration of the triaxiality is mandatory in holistic ice-fluid-propeller simulation because the water confines the ice. The MCNS model can be a good candidate for a holistic ice material model because it can also be used for sea ice, as the two material parameters, the angle of friction

and the cohesion value, can be determined directly from the field measurements using compression and tensile tests.

6 CONCLUSION

In conclusion, our comprehensive experimental investigation involving 18 drop tower tests, each with three repetitions for various interaction velocities, has provided valuable insights into the preliminary drop tower tests with model edges of different thicknesses mimicking propeller-edges. Notably, the 3 mm model edge exhibited variability in failure modes, with instances of splitting rather than the anticipated local crushing. However, the splitting failure mode resulted in the lowest measured forces. The possibility of alternative failure modes in larger specimens will be investigated in the future. While the experiments have yielded meaningful findings for the purpose of future experiments using a scaled propeller, the future setup should incorporate acceleration measurements of the drop hammer, as they offer greater sensitivity in capturing high dynamics and could provide more precise results for larger displacements.

In addition, the paper answers the research question. Can the Mohr-Coulomb Nodal Split model be applied to the numerical investigation of ice-propeller interaction? Answer: Yes, if the MCNS model is further developed to represent the strain-rate dependency at compression and the triaxiality. The presented MCNS model reproduces the maximum measured forces and the recorded behavior in the experiments. Figure 7 and the comparison of Figure 6 with Figure 8 show that the MCNS model with the initial settings is conservative yet realistic for these kinds of simulations. Consequently, we will assess the future experimental setup utilizing propeller edges by simulating the propeller-ice interaction with the initial MCNS model among other possible material formulations for the ice. If the simulations show, that the load transfer of the ice is too high for the propeller edges, the dimensions of the ice specimen can be changed. The structure of the drop tower, the drop hammer, or the foundation will be enforced when future simulations show high stresses or large movements of the structure. Nevertheless, investigations of the meshing method, mesh size (and thus contact stiffness), the plastic strain, the strain-rate dependency, and triaxiality must follow. In the realm of the finite element method this can lead to the derivation of a holistic ice material formulation for ice-propeller interactions.

REFERENCES

Allianz Global Corporate and Specialty (2021). 'Incidents in Arctic Circle waters'. Safety and Shipping Review 2021: 55

Belyashov, V. A.; Shpakov, V. S. (1983). 'On Mechanics of Ice Crushing by Propeller Blades. Ice Mechanics and Physics'. Ice Mechanics and Physics: 21-29.

Belyashov, V. A. (1993). 'An investigation on fracture mechanics and ice loads during cutting freshwater ice by indenters simulating propeller blades. Part 1: Flat horizontal indenters'. International Conference on Port and Ocean Engineering under Arctic Conditions: 3-16. Hamburg, Germany.

Belyashov, V. A. (1995). 'An investigation on fracture mechanics and ice loads during cutting freshwater ice by indenters simulating propeller blades. Part 2: Flat vertical indenters'. International Conference on Port and Ocean Engineering under Arctic Conditions: 18-30. Murmansk, Russia.

Böhm, Angelo Mario; Herrnring, Hauke; von Bock und Polach, Franz. (2022a). 'Data from uniaxial compressive testing of laboratory-made granular ice'. Data in brief **42**: 108236.

Böhm, Angelo Mario; Herrnring, Hauke; von Bock und Polach, Franz. (2022b). 'Splitting-Tests of Laboratory-Made Granular Ice With a Propeller-Like Indenter'. Volume 6: Polar and Arctic Sciences and Technology. ASME 2022 41st International Conference on Ocean, Offshore and Arctic Engineering. Hamburg, Germany.

Böhm, Angelo Mario; Müller, Franciska; Herrnring, Hauke John; von Bock und Polach, Franz. (2023). 'High-speed Impact Drop Tower Tests of Cylindrical Granular Ice Specimens'. International Conference on Port and Ocean Engineering under Arctic Conditions. Glasgow, Scotland.

Gagnon, R.; Andrade, S. L.; Quinton, B.; Daley, C.; Colbourne, B. (2020) 'Pressure distribution data from large double-pendulum ice impact tests'. Cold Regions Science and Technology **175**: 103033

Herrnring, Hauke; Kubiczek, Jan M.; Ehlers, Sören. (2020). 'The ice extrusion test: a novel test setup for the investigation of ice-structure interaction – results and validation'. Ships and Offshore Structures **15** (sup1): 1-9.

Herrnring, Hauke; Ehlers, Sören. (2022). 'A Finite Element Model for Compressive Ice Loads Based on a Mohr-Coulomb Material and the Node Splitting Technique'. Journal of Offshore Mechanics and Arctic Engineering **144** (2): 021601

Herrnring, Hauke. (2023). Experimental and numerical investigation of brittle ice crushing loads. TUHH Universitätsbibliotek. Hamburg, Germany.

Herrnring, Hauke; Kubiczek, Jan M.; Ehlers, Sören; Niclasen, N. O.; Burmann, M. (2017). 'Experimental investigation of an accidental ice impact on an aluminium high speed craft'. C. Guedes Soares, Y. Garbatov (Eds.): Progress in the analysis and design of marine structures. Proceedings of the 6th International Conference on Marine Structures (MARSTRUCT 2017). Lisbon, Portugal.

Hoffmann, Lutz. (1985). 'Impact forces and friction coefficent on the forebody of the german polar research vessel Polarstern'. International Conference on Port and Ocean Engineering under Arctic Conditions. Narssarssuaq, Greenland.

Khan, Aaqib G.; Hisette, Quentin; Streckwall, Hein-

rich; Liu, Pengfei. (2020) 'Numerical investigation of propeller-ice interaction effects'. Ocean Engineering **216**: 107716

Kotras, T.; Humphreys, D.; Baird, A.; Morris, G.; Morley, G. (1987). 'Determination of Propeller-Ice Milling Loads'. Journal of Offshore Mechanics and Arctic Engineering 109 (2): 193-199.

Kujala, Pentti; Jiang, Zongyu; Li, Fang; Lu, Liangliang (2009). ' Long term prediction of local ice loads on the hull of S.A. Agulhas II'. International Conference on Port and Ocean Engineering Under Artic Conditions. Luleå, Sweden.

Lu, Yu; Wu, Chunxiao; Liu, Shewen; Gu, Zhuhao; Shao, Wu; Li, Chuang. (2021). 'Research on Optimization of Parametric Propeller Based on Anti-Icing Performance and Simulation of Cutting State of Ice Propeller'. Journal of Marine Science and Engineering **9**(11): 1247

Müller, Franciska; Böhm, Angelo Mario; Herrnring, Hauke; von Bock und Polach, Franz; Ehlers, Sören. (2023). 'Experimental and Numerical Analysis of Ice Crushing Tests With Different Shaped Ice Specimens'. Volume 6: Polar and Arctic Sciences and Technology. ASME 2023 42nd International Conference on Ocean, Offshore and Arctic Engineering. Melbourne, Australia.

Nickerson, Brendon Mark; Bekker, Anriëtte. (2021). 'Recommendations for regularization in the inverse estimation of ice-induced propeller moments for ice-going vessels'. Cold Regions Science and Technology **192**: 103378

Shadloo, M. S.; Oger, G.; Le Touzé, D. (2016). 'Smoothed particle hydrodynamics method for fluid flows, towards industrial applications: Motivations, current state, and challenges'. Computers & Fluids **136**: 11-34

Soininen, Harri. (1998). 'A propeller-ice contact model'. VTT (VTT publications 343). Espoo, Finland).

Suominen, Mikko. (2018). 'Uncertainty and variation in measured ice-induced loads on a ship hull'. Aalto University. Aalto, Finland.

Suominen, Mikko; Karhunen, Jouko; Bekker, Anriëtte; Kujala, Pentti; Elo, Mikko; von Bock und Polach, Franz. (2013). 'Full-Scale Measurements on Board PSRV S.A.Agulhas II in the Baltic Sea'. International Conference on Port and Ocean Engineering under Arctic Conditions. Espoo, Finland.

Timco, G. W.; Weeks, W. F. (2010). 'A review of the engineering properties of sea ice'. Cold Regions Science and Technology **60** (2): 107-129.

Veitch, Brian J. (1995). 'Prediction of ice contact forces on a marine screw propeller during the propeller-ice cutting process'. Helsinki University of Technology. Helsinki, Finland.

de Waal, R.J.O.; Bekker, A.; Heyns, P. S. (2018) 'Indirect load case estimation for propeller-ice moments from shaft line torque measurements'. Cold Regions Science and Technology **151**: 237-248

Wang, C.; Xiong, W. P.; Chang, X.; Ye, L. Y.; Li, X. (2018). 'Analysis of variable working conditions for propeller-ice interaction'. Ocean Engineering **156**: 277-293.

Wang, Jungyong. (2007). 'Prediction of propeller performance on a model podded propulsor in ice (propeller-ice interaction)'. Memorial University of Newfoundland

Xiong, WeiPeng; Wang, Chao; Wang, ChunHui; Ma, Qing Wei; Xu, Pei. (2020). 'Analysis of shadowing effect of propeller-ice milling conditions with peridynamics'. Ocean Engineering **195**: 106591.

Yang, Dongbao; Liu, Lu; Ji, Shungying. (2023). 'Numerical analysis of interaction between sea ice and propeller based on coupled DEM-FEM model'. Ocean Engineering **268**: 113469

Ye, L. Y.; Wang, C.; Chang, X.; Zhang, H. Y. (2017). 'Propeller-ice contact modeling with peridynamics'. Ocean Engineering **139**: 54-64.

Ye, L. Y.; Guo, C. Y.; Wang, C.; Wang, C. H. (2019) 'Prediction of the dynamic pressure distribution on a propeller blade under ice milling'. Ocean Engineering **188**:106284

Zhou; Wang; Diao; Ding; Yu. (2019). 'Simulation of Ice-Propeller Collision with Cohesive Element Method'. Journal of Marine Science and Engineering **7**(10): 349